Research Article | Vol. 27, No. 3 | 4 Feb 2019 | OPTICS EXPRESS 3217
Optics EXPRESS

Ring artefact reduction via multi-point piecewise linear flat field correction for X-ray computed tomography

JOSEPH LIFTON* AND TONG LIU

Singapore Institute of Manufacturing Technology, Precision Measurements Group, 73 Nanyang Drive, 637662, Singapore
**joe_lifton@simtech.a-star.edu.sg*

Abstract: X-ray computed tomography (XCT) is a well-established method for measuring and inspecting an object's internal structure in a non-destructive manner. Ring artefacts are unwanted high- or low-intensity rings that appear in CT images that influence CT-based measurements. The cause of the subtle ring artefacts found in high-resolution XCT data is found to be due to inadequate flat field detector correction. Therefore, in this work, the usual two-point flat field correction is replaced by a multi-point, piecewise linear flat field correction. The proposed method is shown to increase the signal-to-noise ratio of exemplary CT data by up to 12.1%. Based on the results presented, it is recommended that a minimum of seven open field images should be used for flat field correction.

1. Introduction

X-ray computed tomography (XCT) is used for a wide range of non-destructive measurement and inspection tasks: from bulk porosity measurements for additively manufactured parts [1], to digital archiving of rare and fragile historical objects [2]. Although XCT can achieve sub-micron 3D sampling resolutions, CT image quality can be degraded through the presence of artefacts (artificial features) such as the blurring of fine detail due to geometric misalignment of the CT hardware [3], drift of the X-ray focal spot position [4], thermal variations [5] and grey value variations due to non-linear X-ray attenuation [6–8], in this work CT image quality degradation by so-called ring artefacts is addressed.

Ring artefacts are high and low intensity concentric ring-like features that appear in CT data, they are centered on the object's centre of rotation and superimposed on top of the reconstructed image, see Fig. 1. Ring artefacts are ultimately caused by imperfect X-ray detector pixels, where a perfect pixel displays perfect linearity between input X-ray intensity and output grey value, and all pixels have the same response when subjected to the same input signal. There are many different underlying causes for individual pixels to have imperfect responses, these include defects in the scintillator, photodetector, and the readout electronics, alongside the final assembly of the detector. Additionally, pixel responses may vary due to numerous time dependent drifts, such as thermal drifts and changes in the X-ray spectrum due to beam hardening, or changes in the X-ray spectrum due to pitting of the X-ray target. Irrespective of the source of a pixel's imperfect response, it is desirable to reduce the presence of ring artefacts in CT data, this being the purpose of the present work.

A large body of work exists on ring artefact correction as it is a common artefact in XCT imaging, a review and comparison of methods is given by Anas et al. [9]. Generally speaking there are two approaches to correcting ring artefacts, pre-reconstruction methods and post-reconstruction methods. Pre-reconstruction methods include constructing sinograms from the projection data, a systematically defective pixel will introduce a stripe in the sinogram which can be easily removed by image processing methods, see Rivers et al. [10] for a simple but effective method and Münch et al. [11] for a much more advanced treatment of stripe removal. Post-reconstruction methods typically involve converting CT images into polar

#349564 https://doi.org/10.1364/OE.27.003217
Journal © 2019 Received 2 Nov 2018; revised 13 Dec 2018; accepted 1 Jan 2019; published 30 Jan 2019

Optics EXPRESS

coordinates such that rings are transformed into stripes, these stripes are then removed using various image processing methods, see for example Sijbers et al. [12] who proposed a method that relies on evaluating local grey value statistics to determine if a stripe is present in a given pixel region. Stripe removal methods can only correct ring artefacts caused by pixels that are erroneous throughout a scan, if a pixel response is erroneous for only a portion of a scan then it will not present as a constant stipe in either the sinogram or an unwrapped CT image, this being a limitation of these type of ring artefact correction methods. One very effective method to reduce ring artefacts is to shift the object or detector during scanning such that the object is projected on different regions of the detector during a scan, this averages out the effect of non-uniform detector responses [13], however it has the disadvantage of reducing the spatial resolution of the CT data if the detector or object shifts are not accurately known [14].

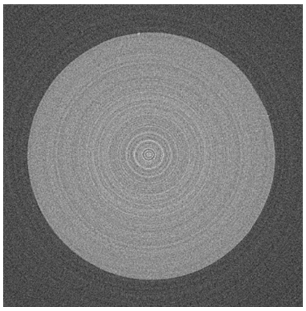

Fig. 1. A CT image displaying severe ring artefacts, the CT image is of a uniform polymer rod.

In this work ring artefacts are addressed through flat field correction, where flat field correction is defined as the pixel-wise correction required such that all pixels have the same grey value output when subject to uniform irradiation [15]. Flat field correction is normally performed by acquiring a bright field and dark field image [16]: a bright field image is the detector output when irradiated by an unobstructed X-ray beam, and a dark field image is the detector output when the X-ray beam is switched off. The flat field correction is normally calculated as follows: let the intensity of a pixel be $I_B(x, y)$ for a bright field image and $I_D(x, y)$ for dark field image, plot these two intensity values against the respective mean detector intensity, denoted μ_B for the bright field image and μ_D for the dark field image, and calculate the gradient and offset of the line that passes through these points: the gradient represents the pixel gain $G(x, y)$ and the intercept represents the pixel offset $O(x, y)$ The pixel specific gain and offset are therefore calculated as follows:

$$G(x,y) = \frac{\mu_B - \mu_D}{I_B(x,y) - I_D(x,y)} \tag{1}$$

$$O(x,y) = \mu_B - G(x,y) I_B(x,y) \tag{2}$$

These pixel-wise gain and offset maps can be applied to the raw detector output $I_R(x, y)$ to give a flat field corrected output $I_C(x, y)$:

$$I_C(x,y) = I_R(x,y) G(x,y) + O(x,y) \tag{3}$$

Example pixel-wise gain and offset images are shown in Fig. 2. The X-ray detector shown in Fig. 2 is a Varian Paxscan 2520 (Varian Medical Systems, CA, USA) flat panel detector with 1480 by 1848 pixels, the pixel size is 0.127 by 0.127 mm, the scintillator is CsI and the receptor is amorphous silicon. This detector is used throughout this work. The gain and offset images clearly show the flat panel detector structure and the variations in the pixel-to-pixel responses.

Optics EXPRESS

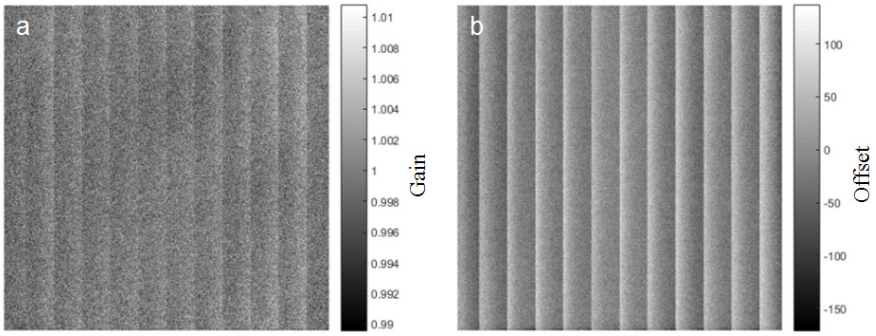

Fig. 2. (a) Image of pixel-wise gain calculated using a bright field and dark field image. (b) Image of pixel-wise offset calculated using a bright field and dark field image.

A more accurate way of estimating the gain and offset values is to conduct a multi-point flat field correction, i.e. using more than two intensities to calculate the gain and offset maps, this is accomplished by changing the X-ray filament current to values between zero and the scan intensity. By measuring more than two intensity levels the gain and offset can be estimated by means of a least squares line, thus improving the accuracy of the estimation of $G(x, y)$ and $O(x, y)$, this approach was evaluated in early work by Seibert et al. [15], in more recent work a polynomial fit was evaluated by Kwan et al. [16] and by Hofmann et al. [17]. Hofmann et al. suggested using piecewise linear interpolation rather than a least squares line or a polynomial function for flat field correction, the piecewise linear correction outperformed both the linear and polynomial correction. Hofmann et al. showed that using piecewise linear interpolation as a basis for flat field correction improves both signal-to-noise ratio (SNR) and contrast sensitivity of X-ray images. Both the work of Hoffmann et al. [17] and Seibert et al. [15] considered the influence of flat field correction on radiographic image quality only, and not CT image quality. Errors in flat field correction are expected to be much more significant for CT image quality than for radiographic image quality since errors will be cumulative due to the summative nature of the filtered backprojection reconstruction algorithm. As such, the main contribution of this work is to study the influence of multi-point piecewise linear flat field correction on CT image quality, particularly for the reduction of ring artefacts.

2. Multi-point piecewise linear flat field correction

The proposed method is implemented as follows: prior to starting a CT scan and after selecting the X-ray settings for a given scan task, open field images (unobstructed X-ray images) are acquired for different X-ray intensities. The X-ray intensity is changed by varying the X-ray source filament current. Using these open field images, a graph is plotted for each detector pixel, this graph compares an individual pixel intensity (x-axis) to the mean detector intensity (y-axis), the resulting trend is approximated by calculating a straight line between two consecutive intensity points, this gives a gain and offset value specific to a range of intensities and a given pixel. This concept is illustrated in Fig. 3(a) for the conventional two-point correction and Fig. 3(b) for the proposed multi-point piecewise linear correction. For the multi-point piecewise linear correction, after a CT scan is conducted the projections are processed, each pixel of each projection is evaluated to check which two intensity points of the flat field correction graph it falls between, the intensity of that pixel is then corrected as per Eq. (3) using the gain and offset previously calculated.

Consider the following example for a single pixel with pixel coordinates x, y: first acquire a series of open field images I_{O1}, I_{O2}, I_{O3}, I_{O4}, next calculate the mean intensity for each open

Optics EXPRESS

field image μ_{O1}, μ_{O2}, μ_{O3}, μ_{O4}, for a single pixel coordinate x, y plot the pixel intensity for each open field image (x-axis) against the mean open field intensity for each image (y-axis), see Fig. 3(b). For each consecutive two points of the graph calculate the line that connects these two points thus giving a gain $G_1(x, y)$, $G_2(x, y)$, $G_3(x, y)$ and an offset $O_1(x, y)$, $O_2(x, y)$, $O_3(x, y)$ for each line. This then gives the proposed multi-point piecewise linear gain and offset maps. To apply this correction to a set of projections the following steps are taken: first load a projection into memory, then for the pixel with coordinates x, y check which two open field intensities the pixel intensity falls between, for example assume the pixel intensity falls between $I_{O2}(x, y)$ and $I_{O3}(x, y)$, in which case the pixel requires correction with gain $G_2(x, y)$, and offset $O_2(x, y)$, apply this correction using Eq. (3) and repeat these steps for all pixels of all projections.

In this work the corrected projections are saved to memory as 32 bit floating numbers and reconstructed in the normal way. All data processing is performed using MATLAB R2015a (MathWorks, MA, USA), the time taken to process a single projection is approximately 1 second, this is predominantly the time taken to read and write the projection data.

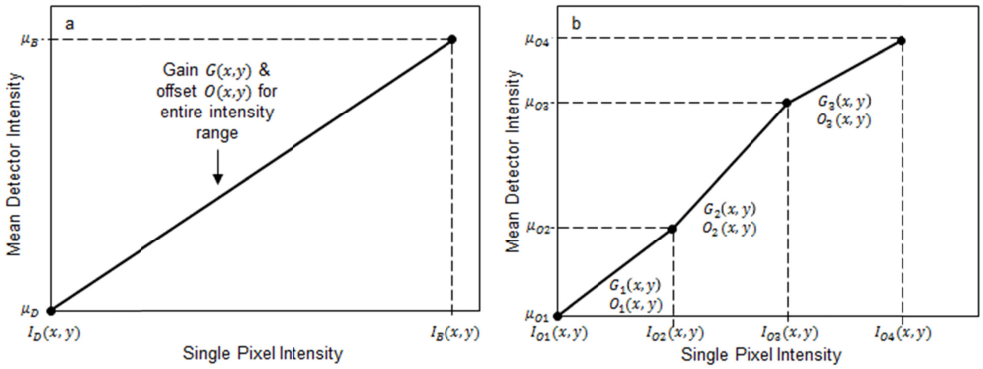

Fig. 3. (a) Illustration of the conventional flat field correction with a single gain and offset derived from a line calculated between two or more open field intensity measurements. (b) Illustration of the proposed multi-point piecewise linear flat field correction: a line is calculated between two consecutive open field intensity measurements to give the gain and offset for this range of intensity values.

3. Number of open field images for flat field correction

A study is conducted to determine how many different intensity open field images should be used for the proposed multi-point piecewise linear flat field correction. CT scans of an aluminium and a nylon cylindrical stepwedge are used for this purpose, see Fig. 4. Different materials are chosen because aluminium and nylon are strongly and weakly X-ray attenuating materials, respectively. Cylindrical stepwedges are used because they present uniform material cross-sections and introduce minimal streaking artefacts so as to isolate the influence of ring artefacts on the grey values. The aluminium stepwedge is scanned with an X-ray source voltage of 110 kV and a current of 10 µA, the nylon stepwedge is scanned with an X-ray source voltage of 90 kV and 15 µA, 1200 projections are acquired for both scans with an exposure time of 1 second.

Prior to scanning, open field images are captured. Each image is generated using a different X-ray intensity, the X-ray intensity is changed by varying the X-ray filament current from the respective scanning current to 0 µA. The noise of each open field image is minimised by averaging 32 frames per measurement. The projections of the aluminium and nylon stepwedges are corrected using flat field corrections calculated with varying numbers of open field images before CT reconstruction.

Optics EXPRESS

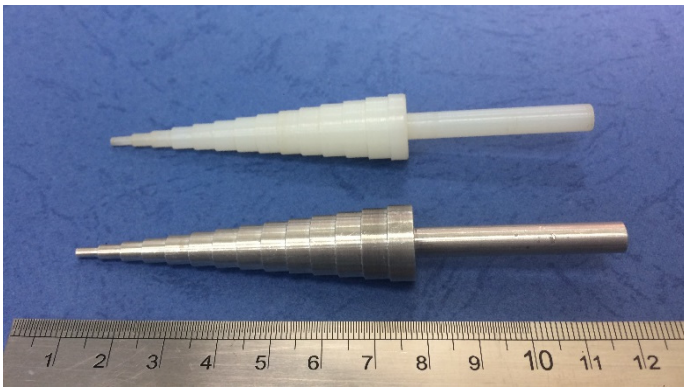

Fig. 4. Photograph of the stepwedges used to assess the influence of number of open field images used for the flat field correction.

The quality of the different flat field corrections is assessed by evaluating the standard deviation of the material grey values of the reconstructed data, this is done by sampling the standard deviation of grey values in a region of interest in the central slice of each data set. If the standard deviation of the grey values decreases, then this indicates less noise and/or reduced ring artefacts.

Figure 5 is a plot of the number of open field images used for the multi-point piecewise linear flat field correction plotted against the standard deviation of the material grey values evaluated from the reconstructed CT data. For both the aluminium and nylon stepwedges it can be seen that as the number of open field images used in the flat field correction increases, the standard deviation of the grey values in the CT data decreases. The standard deviation of the data begins to converge at around 7 open field images for both the aluminium stepwedge and the nylon stepwedge. For the aluminium stepwedge the standard deviation of the material grey values reduces by 4.1%. For the nylon stepwedge the standard deviation of the material grey values decreases by 3.3%.

Based on these results a 7 point piecewise linear flat field is recommended instead of the usual 2-point correction. More than 7 open field images can be used but this may not lead to a significant improvement in ring artefact reduction. These recommendations are further tested in Section 5. For CT measurement tasks that are to be repeated many times it is recommended that a convergence study is conducted as presented in Fig. 5 in order to optimise the number of open field images used in the flat field correction.

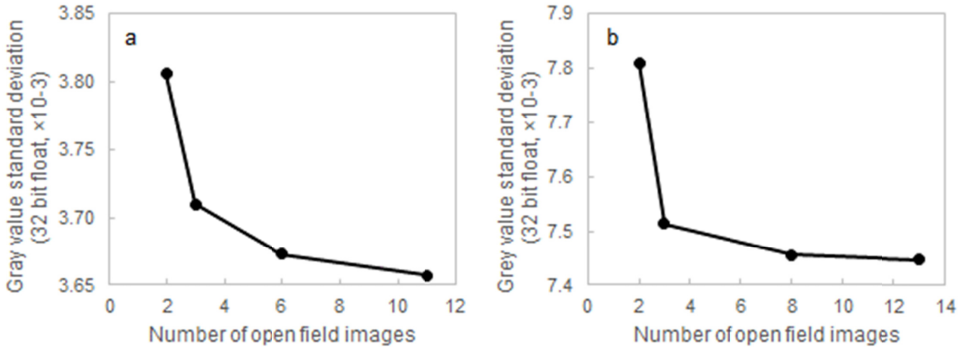

Fig. 5. Influence of the number of open field images used for the multi-point piecewise linear flat field correction on the standard deviation of the material grey values in reconstructed CT data, (a) for the aluminium stepwedge, (b) for the nylon stepwedge.

Optics EXPRESS

4. The influence of flat field correction on the pixel-wise linearity of the detector

The pixel-wise linearity of the detector is evaluated using the standard two-point flat field correction and the proposed multi-point piecewise linear flat field correction. The linearity of each pixel is evaluated by plotting the single pixel intensity against the mean detector intensity for 9 different intensities and then evaluating the coefficient of determination R^2 of the least squares line fitted to this trend. The intensity of the X-ray beam is changed by placing aluminium sheets between the X-ray source and the detector, the sheet thickness is varied from 0 to 4.5 mm in steps of 0.5 mm. Aluminium sheets are used to vary the X-ray intensity because this will not only change the X-ray flux but also the X-ray energy spectrum due to the physical processes of beam hardening and scattering which may cause additional nonlinearities in the pixel response [14,18]. This is a more accurate representation of what happens during a CT scan: i.e. the detected X-ray intensity and the X-ray spectrum change due to the polychromatic attenuation of X-rays by a material object. The multi-point piecewise linear flat field correction is calculated using 11 open field images generated by changing the filament current from 0 to 10 µA in steps of 1 µA, with 32 averaged frames per image.

Pixel-wise linearity maps of the detector evaluated using the two-point flat field correction and the multi-point piecewise linear flat field correction are shown in Fig. 6. When using the two-point flat field correction the linearity clearly varies across the detector, this variation in linearity is quantified by evaluating the standard deviation of the linearity values. The multi-point piecewise linear flat field corrected linearity map shows an improvement compared to the two-point method, a visual inspection of Fig. 6 shows that the linearity map is more uniform. The standard deviation of the two-point flat field corrected linearity map is 4.25e-4 whilst the standard deviation of the multi-point piecewise linear flat field corrected linearity map is 3.29e-4, this constitutes a 22.5% reduction in the standard deviation of linearity values. Clearly the multi-point piecewise linear flat field correction is able to reduce the non-linearity of the detector with respect to X-ray intensity. Notice that there is still some structure visible in the linearity map corrected using the proposed method, thus there is still some room for improvement.

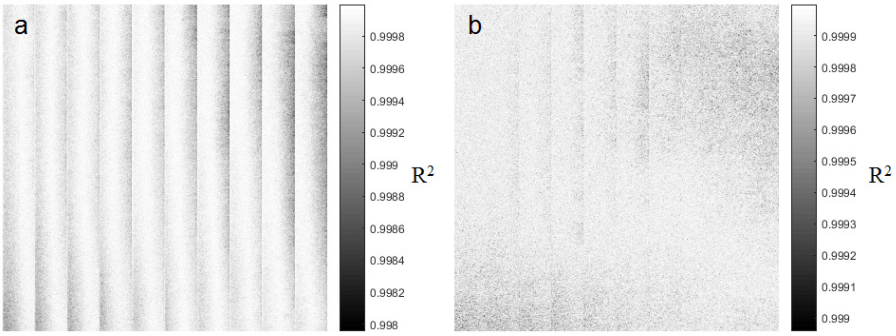

Fig. 6. Pixel-wise linearity of the considered X-ray detector. The linearity is evaluated by plotting the single pixel intensity against the mean detector intensity for 9 different intensities and then evaluating the R^2 of the least squares line fitted to this trend. (a) Two-point flat field correction, standard deviation of 4.25e-4. (b) Multi-point piecewise linear flat field correction, standard deviation of 3.29e-4. Reduction in standard deviation of linearity maps by 22.5%.

5. Application to CT scans of example workpieces

The proposed flat field correction is applied to scans of three example workpieces shown in Fig. 7, these being a porous ceramic filter, a ceramic additively manufactured (AM) cube with

Optics EXPRESS

a repeating internal cellular structure, and a polymer cube with various diameter holes drilled into its faces. These example workpieces represent the variety of objects an X-ray inspection lab may regularly encounter for defect inspection and measurement.

The workpieces are scanned using a YXLON Y.Fox XCT system (YXLON International GmbH, Hamburg, Germany) which features a 160 kV tungsten transmission target X-ray source and a flat panel detector with a CsI scintillator, amorphous silicon photodetector and 1848 by 1480, 0.127 mm pixels. The scan and reconstruction settings for each workpiece are specified in Table 1, all reconstructions are conducted using VGStudio MAX 2.2 (Volume Graphics GmbH, Heidelberg, Germany) using the cone beam filtered backprojection algorithm.

Open field images are acquired prior to CT scanning and are used for the multi-point piecewise linear flat field correction, 32 frames are averaged for each open field image: 13 open field images are used for the ceramic filter, 12 open field images are used for the AM ceramic cube and 13 open field images are used for the polymer cube. The number of open field images used for the flat field correction is chosen based on the scanning X-ray source current: the source current is changed from the scanning current to 0 μA in steps of 1 μA and an open field image acquired at each source current value. For the sake of comparison, the usual 2 point flat field correction is also evaluated, alongside the recommended 7 point piecewise linear flat field correction.

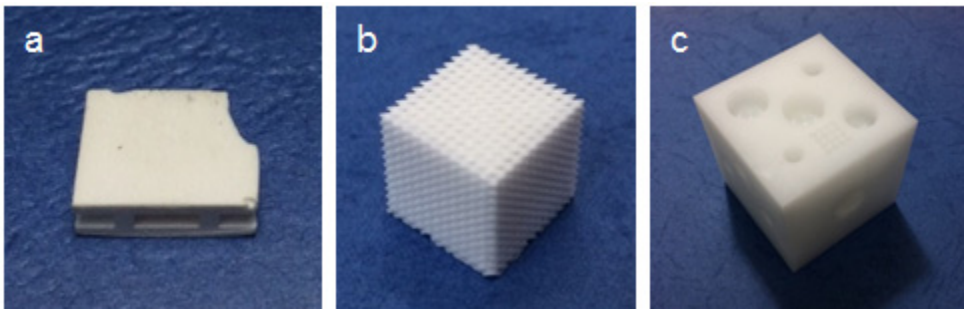

Fig. 7. Three example workpieces (a) porous ceramic filter 1 × 0.5 × 0.3 cm (width × depth × height), (b) ceramic additively manufactured cube with a repeating internal cellular structure 1.2 × 1.2 × 1.2 cm, and (c) polymer cube with various diameter holes drilled into its faces 4 × 4 × 4 cm.

Table 1. X-ray CT scan settings for each workpiece.

	Value		
Parameter	Ceramic filter workpiece	Additively manufactured ceramic workpiece	Polymer workpiece
Source voltage (kV)	100	105	100
Source current (μA)	12	11	12
Detector exposure time (s)	1		
Projection averages	1		
Number of projections	1200	1200	1200
Reconstruction volume voxel resolution *x,y,z*	1024,1024,1024		
Voxel size, (*x,y,z*) (μm)	10, 10, 12	28, 28, 35	75,75,94
Reconstruction filter	Shepp-Logan		
Reconstruction interpolation	Linear		
Reconstruction data type	32 bit floating point		

CT slices for each workpiece before and after application of the proposed multi-point piecewise linear flat field correction are shown in Figs. 8(a) and 8(b) to Figs. 10(a) and 10(b) alongside the regions of interest from which the signal-to-noise ratio (SNR) is evaluated for quantitative image quality comparison. Ring artefacts are clear in all the uncorrected CT

Optics EXPRESS

slices but their presence is reduced after applying the multi-point piecewise linear flat field correction. The CT slices of the ceramic AM and polymer workpieces show two or three prominent ring artefacts within the material region of the image, these arise from clusters of badly corrected pixels whereas the ceramic filter shows much finer ring artefacts dispersed across the entire reconstruction. Irrespective of the types of ring artefacts, they are successfully reduced by the proposed flat field correction.

For the quantitative comparison the SNR increases by 4.8% for the porous ceramic filter workpiece with a 13-point flat field correction, 12.1% for the ceramic AM workpiece with a 12 point flat field correction and 1.5% for the polymer workpiece with a 13 point flat field correction. The 7 point piecewise linear correction also yields a significant SNR improvement compared to the 2-point correction, see Table 2. These results are in agreement with Section 3, in that 7 open field measurements is sufficient to reduce ring artefacts and increase the SNR of the CT data. For the ceramic AM workpiece and the polymer workpiece using more than 7 open field images further increases the SNR. In the case of the ceramic filter more than 7 open field images slightly reduces the SNR, this is likely due to an overcorrection of the data that introduces additional noise to the reconstruction; irrespective of this slight reduction in SNR the ring artefacts are still sufficiently reduced by the 13 point correction as can be seen from Fig. 8(b).

Line profiles for each CT image are shown in Figs. 8(c) to 10(c), these line profiles highlight where rings have been reduced in each CT image and show that the detail in each CT data set has not been compromised as a result of the flat field correction, this being an advantage of the proposed method as it does not require any filtering of the data and therefore avoids loss of spatial resolution.

The difference between the corrected and uncorrected CT slices are shown in Figs. 8(d) to 10(d). Line profiles across the difference images are also shown in Figs. 8(c) to 10(c). The difference images in Figs. 8(d) and 9(d) show that only rings have been modified in the corrected CT image, and that no object detail has been modified. Figure 10(d) however shows that some detail in the object corners has been modified, this is most likely due to an over or under correction by the 2-point flat field correction. The polymer object edges in the projections will give less attenuation than the bulk of the object, these subtle changes in detected X-ray intensity due to the object edges may then be over or under corrected by the coarse 2-point correction, this may be overcome by using a multi-point piecewise linear flat field correction.

Table 2. Summary SNR values for the different workpieces.

Workpiece	SNR with 2 point correction	SNR with 7 point piecewise linear correction	Percentage increase (%)	*N*	SNR with *N* point piecewise linear correction	Percentage increase (%)
Ceramic filter	3.484	3.661	5.1	13	3.652	4.8
Ceramic AM	8.199	9.118	11.2	12	9.195	12.1
Polymer	9.930	10.072	1.4	13	10.078	1.5

Optics EXPRESS

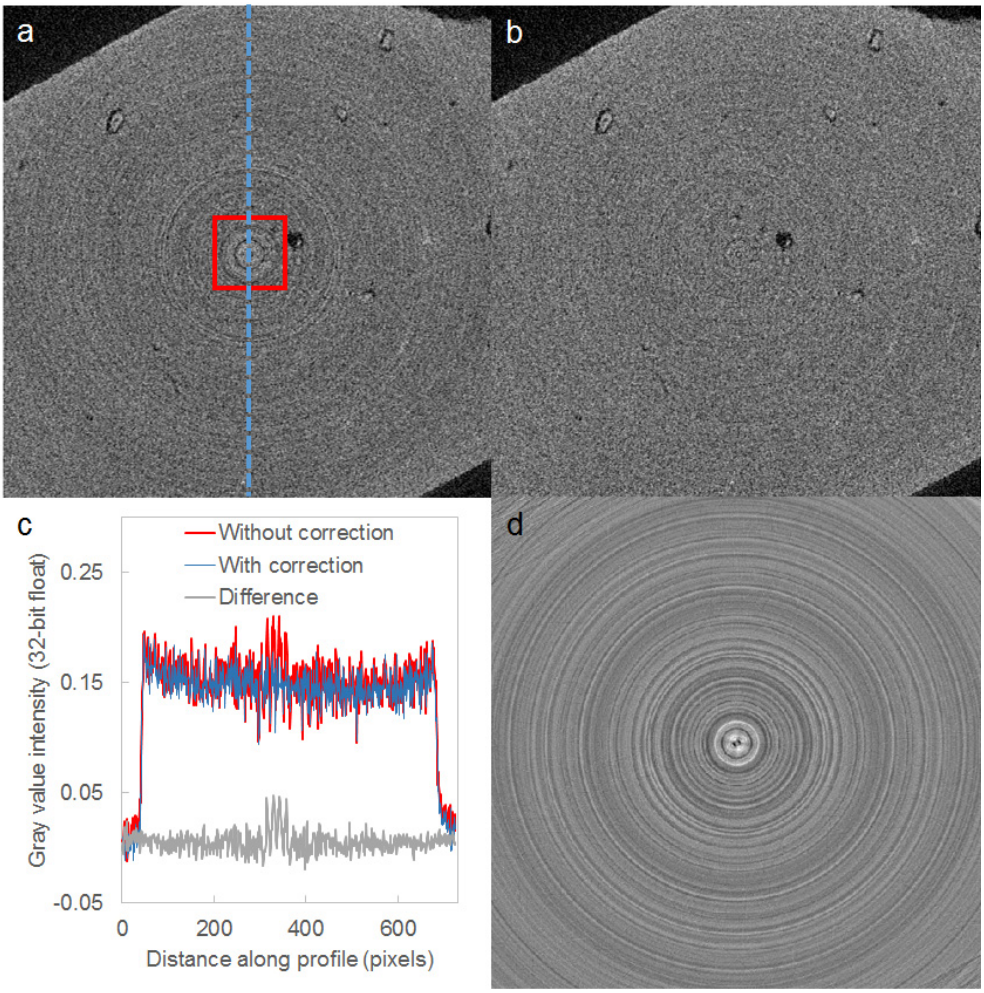

Fig. 8. Central CT images of the porous ceramic filter workpiece reconstructed using a 2-point flat field correction (a) and with a 13 point piecewise linear flat field correction (b). SNR increase of 4.8%, ROI indicated in (a). (c) Plot of line profiles with and without multi-point piecewise flat field correction, line profile position indicated by dashed line in (a). (d) Difference between (a) and (b).

Optics EXPRESS

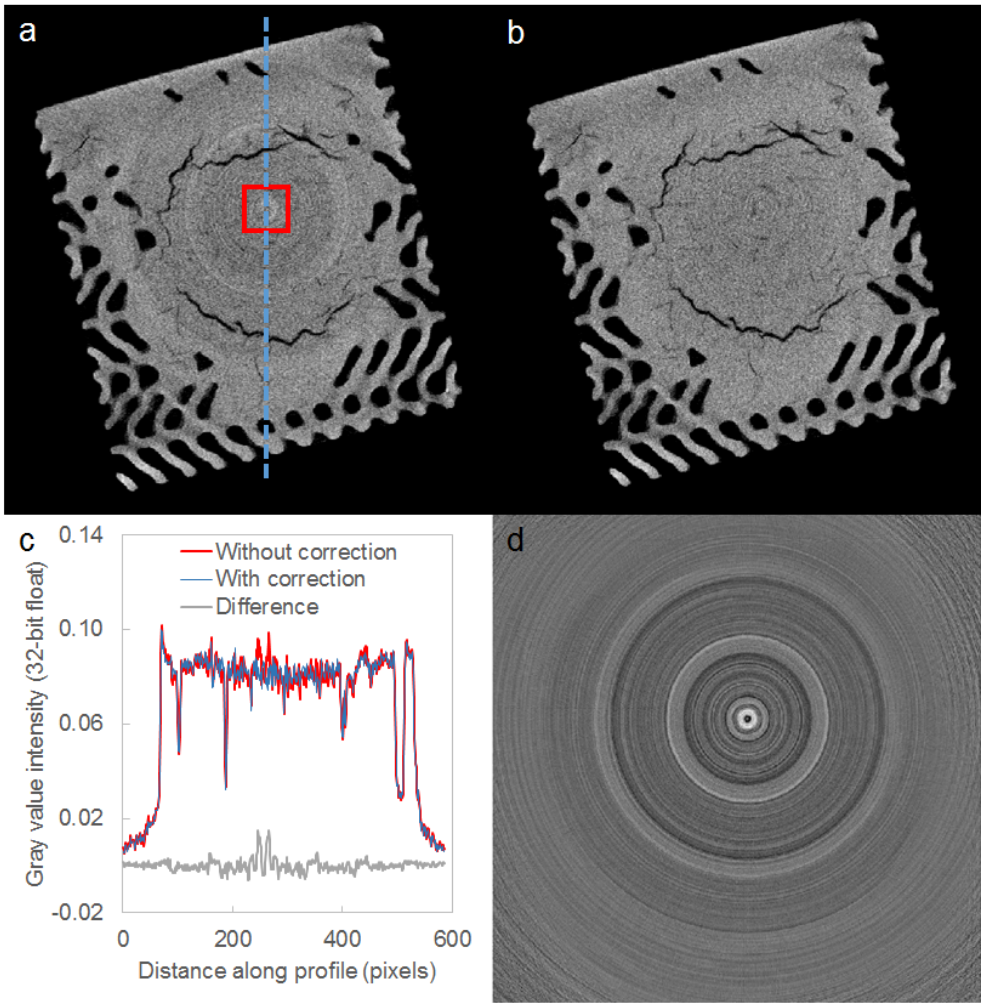

Fig. 9. Central CT images of the AM ceramic cube workpiece reconstructed using a 2-point flat field correction (a) and with a 12 point piecewise linear flat field correction (b). SNR increase of 12.1%, ROI indicated in (a). (c) Plot of line profiles with and without multi-point piecewise flat field correction, line profile position indicated by dashed line in (a). (d) Difference between (a) and (b).

Optics EXPRESS

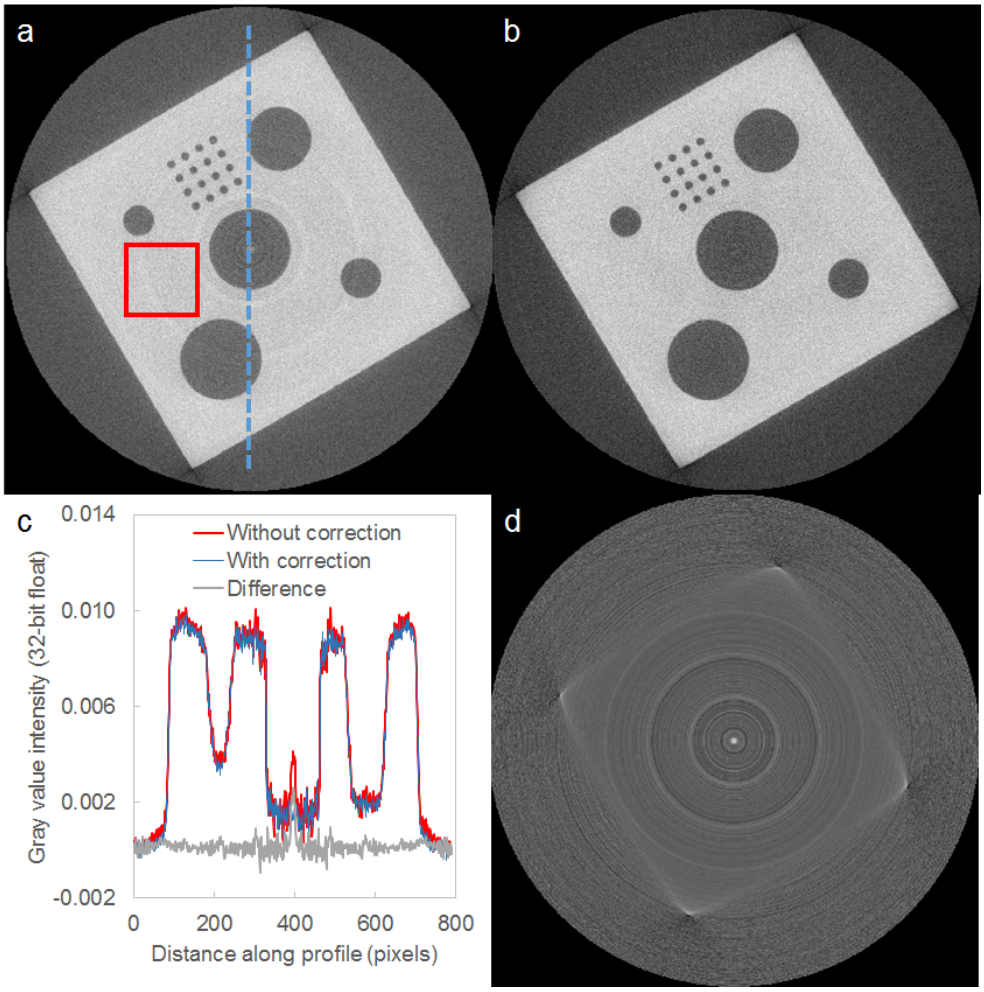

Fig. 10. Central CT images of the polymer cube workpiece reconstructed using a 2-point flat field correction (a) and with a 13 point piecewise linear flat field correction (b). SNR increase of 1.5%, ROI indicated in (a). (c) Plot of line profiles with and without multi-point piecewise flat field correction, line profile position indicated by dashed line in (a). (d) Difference between (a) and (b).

6. Discussion

The proposed method builds upon the early work of Seibert et al. [15] and the more recent work of Hofmann et al. [17], both of whom only considered the influence of flat field correction for radiographic imaging rather than CT imaging. The impact of flat field correction for CT is more profound due to the confounding of pixel errors in tomographic reconstruction.

The proposed method is simple to understand and to implement. It requires additional open field images to be acquired prior to initiating a CT scan, and for the projections to be processed prior to reconstruction, but no system modification or extra apparatus is required. The method has been shown to improve the SNR of CT data evaluated from regions of interest. A visual inspection shows that dominant rings are suppressed whilst the global CT image noise remains similar without visual loss of resolution. It is expected that XCT users scanning low density objects that require very high contrast resolutions will find the proposed method useful.

Optics EXPRESS

A more complicated detector correction method also aimed at ring artefact reduction is described in [14], the method reduces ring artefacts by correcting local variations in the scintillator thickness that are not compensated for by conventional flat field correction. The method shows good performance, but is much more difficult to implement as it requires knowledge of the X-ray source energy spectrum, the scintillator material attenuation coefficients and the scanned object material attenuation coefficients. The requirement for so much *a priori* knowledge on a scan-by-scan basis makes the method impractical for most CT users and researchers. The method proposed in this work is on the other hand simple to implement and requires no specialist equipment or *a priori* knowledge of the scanned object.

7. Conclusions

A multi-point piecewise linear flat field correction method has been proposed and shown to reduce the presence of ring artefacts and to increase the signal-to-noise ratio of CT data. A minimum of seven open field images is recommended for the proposed flat field correction. The method is simple to implement and requires no system modification or additional CT hardware.

References

1. J. A. Slotwinski, E. J. Garboczi, and K. M. Hebenstreit, "Porosity measurements and analysis for metal additive manufacturing process control," J. Res. Natl. Inst. Stand. Technol. **119**, 494–528 (2014).
2. P. L. Rosin, Y.-K. Lai, C. Liu, G. R. Davis, D. Mills, G. Tuson, and Y. Russell, "Virtual recovery of content from x-ray micro-tomography scans of damaged historic scrolls," Sci. Rep. **8**(1), 11901 (2018).
3. F. Noo, R. Clackdoyle, C. Mennessier, T. A. White, and T. J. Roney, "Analytic method based on identification of ellipse parameters for scanner calibration in cone-beam tomography," Phys. Med. Biol. **45**(11), 3489–3508 (2000).
4. W. Sun, S. Brown, N. Flay, M. McCarthy, and J. McBride, "A reference sample for investigating the stability of the imaging system of x-ray computed tomography," Meas. Sci. Technol. **27**(8), 085004 (2016).
5. N. Flay, W. Sun, S. Brown, R. Leach, and T. Blumensath, "Investigation of the focal spot drift in industrial cone-beam x-ray computed tomography," Digital Industrial Radiology and Computed Tomography, Belgium, (2015).
6. J. J. Lifton, A. A. Malcolm, and J. W. McBride, "An experimental study on the influence of scatter and beam hardening in x-ray CT for dimensional metrology," Meas. Sci. Technol. **27**(1), 15007 (2016).
7. J. J. Lifton and S. Carmignato, "Simulating the influence of scatter and beam hardening in dimensional computed tomography," Meas. Sci. Technol. **28**(10), 104001 (2017).
8. J. J. Lifton, A. A. Malcolm, and J. W. McBride, "A simulation-based study on the influence of beam hardening in X-ray computed tomography for dimensional metrology," J. XRay Sci. Technol. **23**(1), 65–82 (2015).
9. E. M. Anas, J. G. Kim, S. Y. Lee, and K. Hasan, "Comparison of ring artifact removal methods using flat panel detector based CT images," Biomed. Eng. Online **10**(72), 72 (2011).
10. M. Rivers, "Tutorial introduction to x-ray computed microtomography data processing," University of Chicago, (1998).
11. B. Münch, P. Trtik, F. Marone, and M. Stampanoni, "Stripe and ring artifact removal with combined wavelet--Fourier filtering," Opt. Express **17**(10), 8567–8591 (2009).
12. J. Sijbers and A. Postnov, "Reduction of ring artefacts in high resolution micro-CT reconstructions," Phys. Med. Biol. **49**(14), N247–N253 (2004).
13. G. R. Davis and J. C. Elliott, "X-ray microtomography scanner using time-delay integration for elimination of ring artefacts in the reconstructed image," Nucl. Instr. and Meth. in Phys. Res. A, **394**(1–2), 157–162 (1997).
14. W. Vågberg, J. C. Larsson, and H. M. Hertz, "Removal of ring artifacts in microtomography by characterization of scintillator variations," Opt. Express **25**(19), 23191–23198 (2017).
15. J. A. Seibert, J. M. Boone, and K. K. Lindfors, "Flat-field correction technique for digital detectors," SPIE Conference on Physics of Medical Imaging, San Diego, California, (1998).
16. A. L. C. Kwan, J. A. Seibert, and J. M. Boone, "An improved method for flat-field correction of flat panel x-ray detector," Med. Phys. **33**(2), 391–393 (2006).
17. T. Hofmann, J. Claussen, F. Nachtrab, I. Bauscher, and N. Uhlmann, "Linearity of flat panel x-ray detectors and comparison of non-linear correction algorithms," International Symposium on Digital Industrial Radiology and Computed Tomography, Berlin, Germany, (2011).
18. D. W. Davidson, C. Fröjdh, V. O'Shea, H.-E. Nilsson, and M. Rahman, "Limitations to flat-field correction methods when using an X-ray spectrum," Nucl. Instr. and Meth. in Phys. Res. A, **509**(1 – 3), 146–150 (2003).